CrossMark

ORIGINAL PAPER

Viscosity and haemodynamics in a late gestation rat feto-placental arterial network

Nikhilesh Bappoo[1,2] · **Lachlan J. Kelsey**[1,2] · **Louis Parker**[1,2] · **Tim Crough**[3] ·
Carmel M. Moran[4] · **Adrian Thomson**[4] · **Megan C. Holmes**[4] · **Caitlin S. Wyrwoll**[3] ·
Barry J. Doyle[1,2,4]

Abstract The placenta is a transient organ which develops during pregnancy to provide haemotrophic support for healthy fetal growth and development. Fundamental to its function is the healthy development of vascular trees in the feto-placental arterial network. Despite the strong association of haemodynamics with vascular remodelling mechanisms, there is a lack of computational haemodynamic data that may improve our understanding of feto-placental physiology. The aim of this work was to create a comprehensive 3D computational fluid dynamics model of a substructure of the rat feto-placental arterial network and investigate the influence of viscosity on wall shear stress (WSS). Late gestation rat feto-placental arteries were perfused with radiopaque Microfil and scanned via micro-computed tomography to capture the feto-placental arterial geometry in 3D. A detailed description of rat fetal blood viscosity parameters was developed, and three different approaches to feto-placental haemodynamics were simulated in 3D using the finite volume method: Newtonian model, non-Newtonian Carreau–Yasuda model and Fåhræus–Lindqvist effect model. Significant variability in WSS was observed between different viscosity

models. The physiologically-realistic simulations using the Fåhræus–Lindqvist effect and rat fetal blood estimates of viscosity revealed detailed patterns of WSS throughout the arterial network. We found WSS gradients at bifurcation regions, which may contribute to vessel enlargement, and sprouting and pruning during angiogenesis. This simulation of feto-placental haemodynamics shows the heterogeneous WSS distribution throughout the network and demonstrates the ability to determine physiologically-relevant WSS magnitudes, patterns and gradients. This model will help advance our understanding of vascular physiology and remodelling in the feto-placental network.

1 Introduction

The placenta is a transient organ which develops during pregnancy to support healthy fetal growth and development. Fundamentally, the placenta serves to secrete hormones and exchange nutrients and waste between the mother and fetus. Inherent to placental function is the appropriate development of complex vascular networks. This is achieved by an expansive villous structure within the placenta which consists of an extensively branched network of fetal vessels; by term, the capillary network is greater than 500 km in length and 15 m^2 in surface area (Burton and Jauniaux 1995). The villi are bathed in maternal blood, and thus fetal and maternal circulations remain distinct. While the fetal capillary network (herein referred to as feto-placental vasculature) is essential for metabolic exchange between the mother and the fetus, it is also a key determinant of the expansion of the placental villous tree. Disruption to the elaboration of the feto-placental

✉ Barry J. Doyle
  barry.doyle@uwa.edu.au

1 Vascular Engineering Laboratory, Harry Perkins Institute of Medical Research, Perth, Australia

2 School of Mechanical and Chemical Engineering, The University of Western Australia, Perth, Australia

3 School of Human Sciences, The University of Western Australia, Perth, Australia

4 Centre for Cardiovascular Science, University of Edinburgh, Edinburgh, UK

Springer

vasculature has profound implications for placental development and function, and ultimately, fetal growth, pregnancy outcome and health in later life. Thus, deficiencies in feto-placental vessel formation, remodelling and growth impede blood flow, impair gas and nutrient transport to the fetus and can ultimately lead to fetal intrauterine growth restriction (IUGR) (Roberts and Post 2008). IUGR occurs in 5–10% of pregnancies (Zhang et al. 2015) and has serious implications for both short and long-term health outcomes. Understanding the mechanisms underlying placental vascular elaboration is therefore vital for devising preventive, diagnostic and therapeutic measures to improve the quality of fetal development.

The similarities between human and rodent placentas make the rodent a useful experimental model for understanding human placental development and function. Comparative studies of rodent and human placenta reveal striking similarity in cell types, structure, haemodynamics and gene expression (Georgiades et al. 2002). Furthermore, the invasiveness and spiral artery development of the rat placenta makes it an especially analogous model of the human placenta (Soares et al. 2012). The site of maternal–fetal exchange in the rodent is the highly vascular labyrinth zone, which consists of an elaborate fetal vascular tree. As described in Georgiades et al. (2002), in both the rodent and human species, umbilical vessels supply the discoid-shaped placenta centrally from which chorionic arteries then branch across the fetal-facing surface of the placenta. In both rodents and human placentas, feto-placental arteries branch deeply into the exchange region of the placenta. While the structural appearance of the feto-placental arterial tree in both species is similar, the primary difference is that humans have ∼20 feto-placental arterial networks, compared to one network in the rodent (Georgiades et al. 2002). However, rodent feto-placental vascular casts have been informative for understanding how feto-placental vascularity informs fetal growth over pregnancy and the effects of environmental perturbation during pregnancy (Georgiades et al. 2002; Rennie et al. 2014; Yang et al. 2010).

Research on feto-placental vessel development has been strongly focused on genetic, molecular and environmental regulation, with little consideration given to biomechanical factors such as shear stress, which is known to affect cellular processes involved in vessel development (Burton et al. 2009). Haemodynamic shear stress and subsequent endothelial function is an important regulator of endothelial nitric oxide synthase that controls nitric oxide, with feto-placental blood flow during gestation heavily reliant on nitric oxide. For a thorough review on the importance of shear stress and nitric oxide production in the placental artery endothelial cells, the nitric oxide reader is referred to Sprague et al. (2010).

Despite the importance of shear stress in feto-placental arteries, previous investigations have been limited in their approach. This is in part due to technical challenges to visualise the feto-placental network in 3D and to assess in vivo microvascular blood flow. Gordan et al. (2007) studied idealised human intra-placental vessels, whereas Bernard et al. (2013) created a 3D model of the first bifurcation of a human placenta and reported velocities and pressure. Others have focussed on oxygen transport in the human placenta capillaries and terminal villi (Pearce et al. 2016; Plitman Mayo et al. 2016). In contrast, the entirety of rodent placental vasculature can be imaged. Recently, 2D imaging techniques of rodent placentas have been replaced by micro-computed tomography (μCT) to acquire 3D images of vascular casts taken from the feto-placental vasculature (Yang et al. 2010). Geometries can be reconstructed through segmentation techniques and then used to comprehensively investigate developmental and functional changes resulting from environmental stressors (Detmar et al. 2008; Rennie et al. 2011; Yang et al. 2010), which is not feasible in human.

Reconstructed μCT 3D vascular networks can additionally be used for computational haemodynamic analyses and help investigate the importance of in vivo mechanical forces on placental development and function. Recent computational models have used rodent vascular networks to examine pressure distributions, shear stresses and velocities in either full arterial networks reconstructed from imaging but with idealised cross sections (Rennie et al. 2011; Yang et al. 2010) or synthetic geometries based on average dimensions (Clark et al. 2015). Despite this excellent prior work, there are no 3D data on the shear stresses within feto-placental arteries, in particular, the distribution and gradient of shear stresses within specific arterial segments and at branch regions. Such data will help further our understanding of oxygen and nutrient exchange in the fetal capillaries as well as the structural development of the entire network itself during gestation.

Therefore, this study aims to develop a framework for the first large scale 3D haemodynamic model of a late gestation rat feto-placental arterial network. Computational fluid dynamics (CFD) was applied to a substructure of the feto-placental vasculature along with realistic assumptions and rheological properties that account for the Fåhræus–Lindqvist effect. Shear stress in the network was computed and compared between different approaches to blood viscosity.

2 Methods

2.1 Animal model and feto-placental arterial casting

In this study we used a single Nulliparous Wistar rat that was part of a larger study group, with rats (6–8 weeks old) supplied by the Animal Resources Centre (Murdoch, Australia). All procedures involving the use of animals were conducted

after approval by the Animal Ethics Committee of The University of Western Australia (AEC number RA/3/100/1300). Rats were maintained in 12:12 light/dark cycle, and food and water were supplied *ad libitum*. Rats were mated, and pregnancy was confirmed by the presence of spermatozoa (designated day 1 of pregnancy, E1). To create arterial casts, dams were anaesthetised with isoflurane/nitrous oxide at E22. Uteri were collected via a midline abdominal incision, feto-placental units dissected and immediately immersed into ice-cold (2–3 °C) phosphate-buffered saline (PBS) for 20 min to induce fetal anaesthesia. Individual feto-placental vascular trees were cleared of blood by perfusion of warm 2% xylocaine (Attane, Bomac, NSW, Australia) in 0.9% sodium chloride (Baxter, Deerfield, IL, USA) and 100 IU heparin/ml (Sigma-Aldrich, St. Louis, MO, USA) into the umbilical artery through a double-lumen glass micropipette. Casting of the feto-placental vasculature was then performed through the perfusion of Microfil® (Carver, MA, USA) based on a method previously developed (Adamson et al. 2002; Whiteley et al. 2006). The vascular cast was left to solidify within the intact placental tissue (see Fig. 1a).

2.2 Scanning feto-placental arterial casts

The cast was immersed in PBS, stabilised in a plastic vial and scanned using μCT (Xradia 520 Versa X-ray Microscope, Xradia 520 XRM, ZEISS, Oberkochen, Germany). To accommodate for the discoid placental structure (∼13.5 mm diameter × 6 mm height), scanning was performed using a novel wide field mode that stitches a set of two normal sized 2D images together horizontally (normal mode tomography = 1K × 1K voxels; wide field mode = 2K × 1K voxels). The desired field of view (FOV) is then shared across two normal images at the same resolution that a normal scan could achieve in half the FOV. Whole placental scanning achieved a resolution of ∼7.1 μm with a scan time of about 15 hours. Data were then exported in DICOM format. Example resulting μCT data are shown in Fig. 1b.

2.3 3D reconstruction and geometry processing

We used Mimics v18 (Materialise, Belgium) to reconstruct the μCT data. Thresholding and region growing helped to segment the arterial structure and remove artefacts, with smaller defects removed manually using 3-matic v10 (Materialise, Belgium). Once reconstructed into 3D, we used a first order Laplacian smoothing algorithm to reduce the noise on the reconstructed outer surface and lumen interior. Laplacian smoothing is a widely used algorithm to smooth a polygonal mesh and works by reducing the distance between vertices in a mesh, where the smoothing factor controls the distance. Here, we used a smoothing factor of 0.7 and ran the algorithm for ten iterations. The resulting geometry is shown in Fig. 1c.

The number of vessels in a vascular structure influences the computational size of the problem as more vessels mean more computational elements. In order to reduce the size of the physical model for CFD, we selected a sub-volume approximately 32% the size of the entire geometry (see dashed box in Fig. 1d). We deemed this appropriate as this sub-volume captures the typical geometry of the region without the need to simulate the entire network. A robust CFD geometry requires the inlet and outlet surfaces to be perpendicular to the direction of flow so that these boundaries do not influence flow in the region of interest. Therefore, we created centrelines in Mimics before following each branching vessel downstream until its border was no longer clearly visible on the μCT; typically near the capillary bed. We then cut each vessel perpendicular to the centreline in this area (see Fig. 1e–f). Our final processed geometry contained one inlet through the umbilical artery and 89 vessel outlets, which was then exported in stereolithography (.stl) format for further use (see Fig. 1g).

2.4 Computational fluid dynamics

2.4.1 Meshing

We used STAR-CCM+ (v11.06, Siemens, Berlin) to create our computational meshes. Each mesh consisted of a core of polyhedral elements and layers of prisms in the near wall boundary layer. Polyhedral meshes are more efficient than tetrahedral meshes; they generate four times fewer cells, use half the memory and approximately one tenth of the computing time when calculating the same solution (Spiegel et al. 2011). We began by remeshing the surface based on the relative average radius of the vessel so that smaller vessels contained more elements. We determined the approximate total thickness of the prism layer based on the local vessel radius, with the prism thickness defined as 10% of the average local diameter. The stretching factor S of each prism layer was calculated such that the thickness of the innermost layer was double the size of the next layer, according to Eq. (1), where n is the number of prism layers. We then created a polyhedral core based on a constant element growth rate of 1.0.

$$S = 2^{\left(\frac{1}{n-1}\right)} \tag{1}$$

The different element types and regional mesh refinement are shown in Fig. 1j, k. We also included entrance and outlet lengths 200 μm long to reduce the impact of inlet and outlet boundary conditions on flow within the domain of interest. This length was verified through simulations to ensure
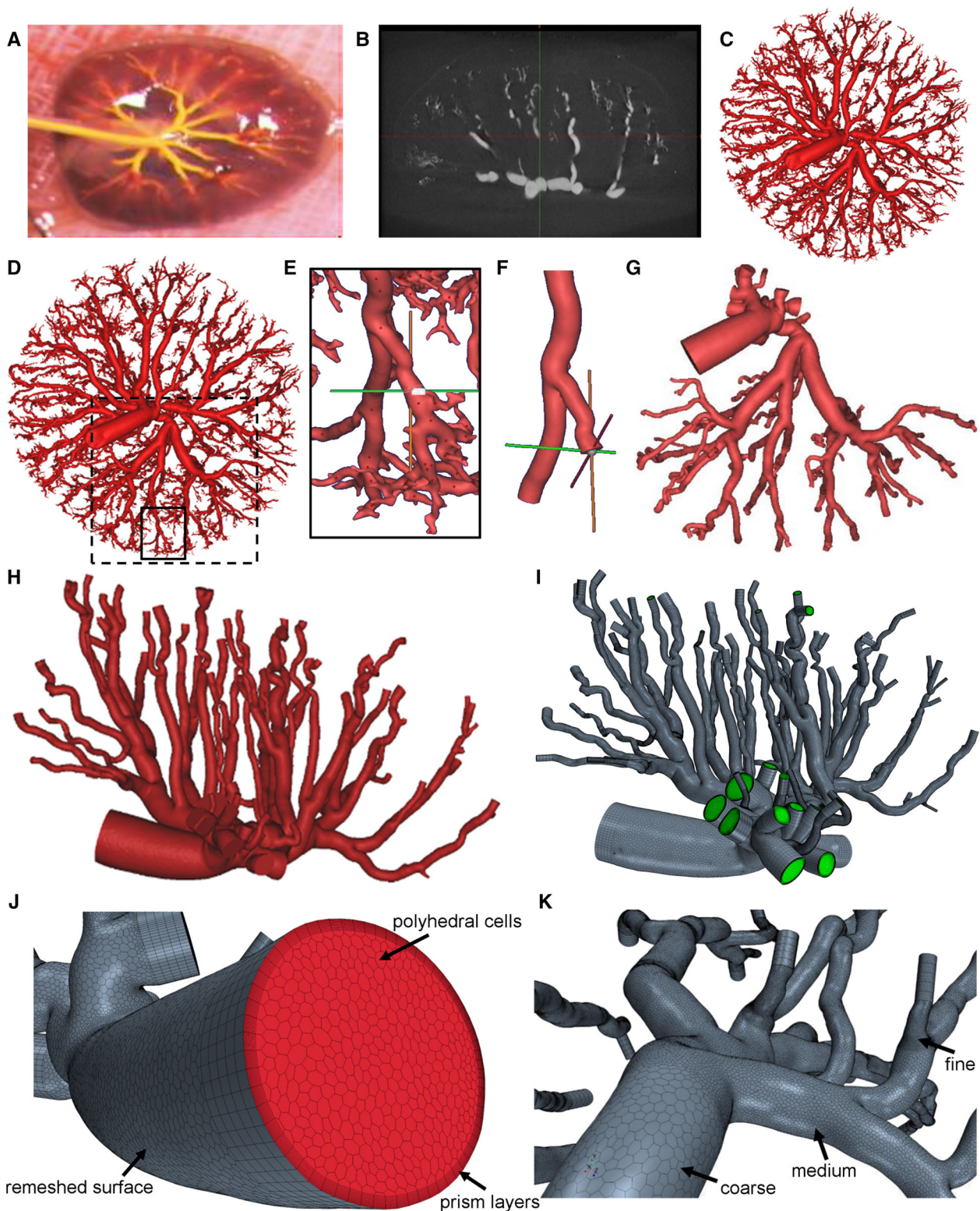
Fig. 1 **a** Microfil cast of the feto-placental unit in situ, **b** example μCT image, and **c** complete 3D reconstruction before further processing. **d** Complete feto-placental network with highlighted region **e** showing the method used to trim vessels perpendicular to the centreline (**f**). **g** Final 3D geometry used for modelling (approximate geometry shown in dashed box in part **d**). Figures **a–g** are shown from above. **h** Final 3D geometry shown from sagittal view and **i** mesh including entrance/exit lengths with outlet faces shown in *green*. **j** Mesh at entrance to umbilical artery (inlet) showing prism layers and polyhedral cells, and **k** local mesh refinement based on local vessel diameter. 'Coarse', 'medium' and 'fine' refers to the mesh density

a developed flow entered and exited the feto-placental network.

2.4.2 Grid convergence

To determine the optimum level of mesh refinement, we tested three mesh densities (coarse, medium and fine) and three different numbers of layers of prism elements. We used the Grid Convergence Index (GCI) (Celik et al. 2008; Roache 1994) to quantify the discretisation error between meshes. We doubled the polyhedral mesh density as well as the number of prism layers until the GCI was <1%. To determine the GCI, we used the same boundary conditions as below, with viscosity accounting for the Fåhræus–Lindqvist effect. Our final computational mesh contained approximately 7 million cells with 12 layers of prism elements.

2.4.3 Umbilical artery velocity measurement

For the inlet condition, we measured the velocity using high-frequency Doppler ultrasound in the umbilical arteries of six late gestation rats (gestation day 22). In vivo ultrasound assessment was performed by using a Vevo 770 ultrasound biomicroscope (Visualsonics) with a RMV710B 25 MHz centre-frequency transducer. Pregnant rats were anaesthetised with 2–3% isoflurane, and body temperature was maintained between 36.5 and 37.5°C. Abdominal body hair was removed. Fetal-placental units were imaged over 45 min, with a minimum of six units analysed in each pregnancy. Blood velocity within the umbilical artery was measured and images were recorded for offline analysis. We determined the average peak systolic velocity to be 136.33 mm/s and this value was used throughout the steady-state simulations.

2.4.4 Boundary conditions and solution parameters

To simulate the blood flow through the network, we solved the 3D incompressible Navier–Stokes and continuity equations using STAR-CCM+. As the system was assumed to be closed and the conservation of mass was enforced, we used Murray's law to determine the branching split ratios which were applied to the mass flow calculations at the outlets. As such, the mass flow at an outlet, i, is equal to the cube of the outlet diameter (d_i^3) divided by the domain wide sum of the cube of each outlet diameter (d_j), multiplied by the inlet mass flow. This is shown by Eq. (2), where N = number of outlets.

$$\text{mass flow}_i = \text{inlet mass flow} \times \frac{d_i^3}{\sum_{j=1}^{N} d_j^3} \qquad (2)$$

We assumed zero velocity (no-slip condition) at all the rigid walls in the model. The flow was assumed laminar throughout as the Reynolds number was low ranging from about 5 in the small bifurcations to 45 in the largest vessel (umbilical artery). Residual convergence criteria (the residual root-mean-square error of continuity equations) was set to 10^{-4} of the starting residual.

2.4.5 Blood viscosity and the Fåhræus–Lindqvist effect

We assessed the resulting differences in haemodynamics between (a) Newtonian model, (b) non-Newtonian model, and (c) one that accounted for the Fåhræus–Lindqvist effect (Fåhræus and Lindqvist 1931) in the microvasculature.

It is difficult to collect rat fetal blood for rheological analysis which results in a scarcity of data in the literature. We reviewed previously published work (Honda et al. 2008; Linderkamp 2004; Linderkamp et al. 1984; Riopel et al. 1982) to investigate the relationship between available human maternal and fetal blood properties and the relevance of haematocrits, measurement conditions (shear rate) and time of pregnancy. We found a constant ratio of neonate to maternal blood viscosities in humans, which was assumed to be comparable in rats. The ratio was applied to available late gestation rat blood data to estimate fetal blood properties relevant to the feto-placental arterial network. A detailed description can be found in the *Supplementary Data*.

In model (a), the Newtonian model, blood was assumed incompressible with a human blood density of 1050 kg m^{-3} analogous to rat blood density (Vitello et al. 2015). In humans, the dynamic whole blood viscosity and plasma viscosity are 3.5 and 1.2 mPa s, respectively. Here, we estimated the dynamic whole blood viscosity and plasma viscosity for rat fetal blood to be 5.14 and 1.14 mPa s, respectively (see *Supplementary Data*).

In model (b), the non-Newtonian model, we implemented the Carreau–Yasuda viscosity model (Eq. 3). The dynamic viscosity μ was calculated where μ_∞ and μ_0 are the values of the dynamic viscosity at infinite and zero shear rate, respectively, λ is the time constant associated with the dynamic viscosity changes with shear rate $\dot{\gamma}$ and n is the power law index.

$$\mu(\dot{\gamma}) = \mu_\infty + (\mu_0 - \mu_\infty)\left(1 + (\lambda\dot{\gamma})^a\right)^{\frac{n-1}{a}} \qquad (3)$$

Appropriate rat blood properties were applied to the Carreau–Yasuda model with $\mu_\infty = 5.14$ mPa s (from our approximations) and $\mu_0 = 0.25$ Pa s, $\lambda = 25$ s, $n = 0.25$ and $a = 2$ taken from the literature (Lecarpentier et al. 2016). We then compared the differences in viscosity and resulting haemodynamics (see *Supplementary Data*).

In model (c), we accounted for the Fåhræus–Lindqvist effect using the mathematical model from Pries et al. (1996),

shown in Eq.(4–6).

$$\mu\left(D, H_D\right) = \frac{\mu}{\mu_{\text{plasma}}}$$

$$= \left[1 + \left(\mu_{0.45} - 1\right) \cdot \frac{\left(1 - H_D\right)^C - 1}{\left(1 - 0.45\right)^C - 1} \cdot \left(\frac{D}{D - 1.1}\right)^2\right]$$

$$\cdot \left(\frac{D}{D - 1.1}\right)^2 \tag{4}$$

Where $\mu_{0.45}$ is the relative blood viscosity for a fixed haematocrit H_D of 0.45 given by Eq. (5).

$$\mu_{0.45} = 6e^{-0.085D} + 3.2 - 2.44e^{-0.06D^{0.645}} \tag{5}$$

D is the vessel diameter, and C describes the shape of viscosity dependence on the haematocrit via Eq. (6).

$$C = \left(0.8 + e^{-0.075D}\right) \cdot \left(-1 + \frac{1}{1 + 10^{-11} \cdot D^{12}}\right)$$

$$+ \frac{1}{1 + 10^{-11} \cdot D^{12}} \tag{6}$$

To implement this model, firstly, a wall distance function was used to compute the distance of local points through the geometry. We obtained a gradient representation of the wall to lumen centreline distance on a very fine polyhedral mesh, where polyhedral cells were approximated as spheres with a $cellsize = 1.2407 \cdot \sqrt[3]{v}$ where v is volume of sphere. Local radii r were then calculated as $r = w + 0.5 \cdot cellsize$, where w is wall distance. This enabled the calculation of local diameters and relative viscosity (μ_{rel}) throughout the 3D geometry.

The distribution of blood viscosity at different diameters was plotted and compared with previous physical measurements (Pries et al. 1996). The dynamic viscosity (μ) was calculated by multiplying the relative viscosity by the plasma viscosity, and the local viscosities were visualised. As before, the rat plasma blood viscosity was assumed at 1.14 and 1.2 mPa s for human plasma blood viscosity. We used a haematocrit of 45% for human blood (Pries et al. 1996) and 31.7% for late pregnancy rat blood (Honda et al. 2008).

2.4.6 Data analysis

We measured the biomechanical factors thought to affect placental blood flow, development, function and pathology: viscosity, velocity and WSS. Viscosity and WSS distributions were compared for the different viscosity models, and percentage differences between the models were calculated and locally represented on the geometry. In each comparison of viscosity, the percentage difference in dynamic viscosity of the Newtonian or Non-Newtonian model is compared to the Fåhræus–Lindqvist model.

3 Results and discussion

3.1 Feto-placental vascular geometry

The entire geometry was 10.6 mm³ in volume and 3380 mm² in surface area. The sub-volume used for CFD was approximately 32% of the entire network's volume comprising of 17% of the surface area. The branching of intra-placental arteries within the sub-volume displayed a large distribution of diameter measurements ranging from 27 µm at the outlets nearing the capillaries, to 756 µm in the umbilical artery (see *Supplementary Data*)

### 3.2 Viscosity in the feto-placental vasculature

Dynamic viscosity decreases with diameter causing the red blood cells to flow centrally within the lumen, leaving a cell-free layer of plasma at the wall with a viscosity much lower than that of the bulk blood. This plasma layer becomes narrowed in the smaller vessels, further reducing the dynamic viscosity at the wall. Figure 2a shows the dynamic viscosity throughout the network when adjusted for the Fåhræus–Lindqvist effect.

We adjusted the haematocrit concentrations to compare with the in vivo data (Lipowsky et al. 1978, 1980; Pries et al. 1994) presented in Pries et al. (1996). We found good agreement; however, we observed earlier inflections in viscosities (see Fig. 2b). Differences could be due to the corrective terms and constants used. Furthermore, the mathematical model assumes a core red cell layer modelled as a rigid body surrounded by a plasma cell-free layer which mostly accounts for the drop in viscosity. We also compared our data with Malek et al. (2015) who implemented the Fåhræus–Lindqvist effect in the human retinal microvasculature. We found very good agreement in each of the haematocrit concentrations investigated and plasma viscosity of 1.2 mPa s (see Fig. 2c). Yang et al. also implemented the Fåhræus–Lindqvist effect into their model and found viscosity to be 2.8 mPa s in vessels with 43 µm diameter. This agrees well with our findings.

The assumption of the core as a rigid body detracts from the physical behaviour of blood as a multi-phase fluid. The actual width of the cell-free plasma layer is dependent on the biomechanics of individual red blood cells which exhibit dynamic motion. There has been little focus on the interaction of red blood cells with each other and the walls, which would alter the assumption of the rigid core body. Although this assumption would hold for smaller arteries, mathematical models of higher complexity need to be considered in larger microvessels.

The Newtonian model produced a constant absolute viscosity throughout the geometry (as expected), while the Carreau–Yasuda viscosity displayed a more heterogeneous distribution of higher magnitude viscosities. The differ-
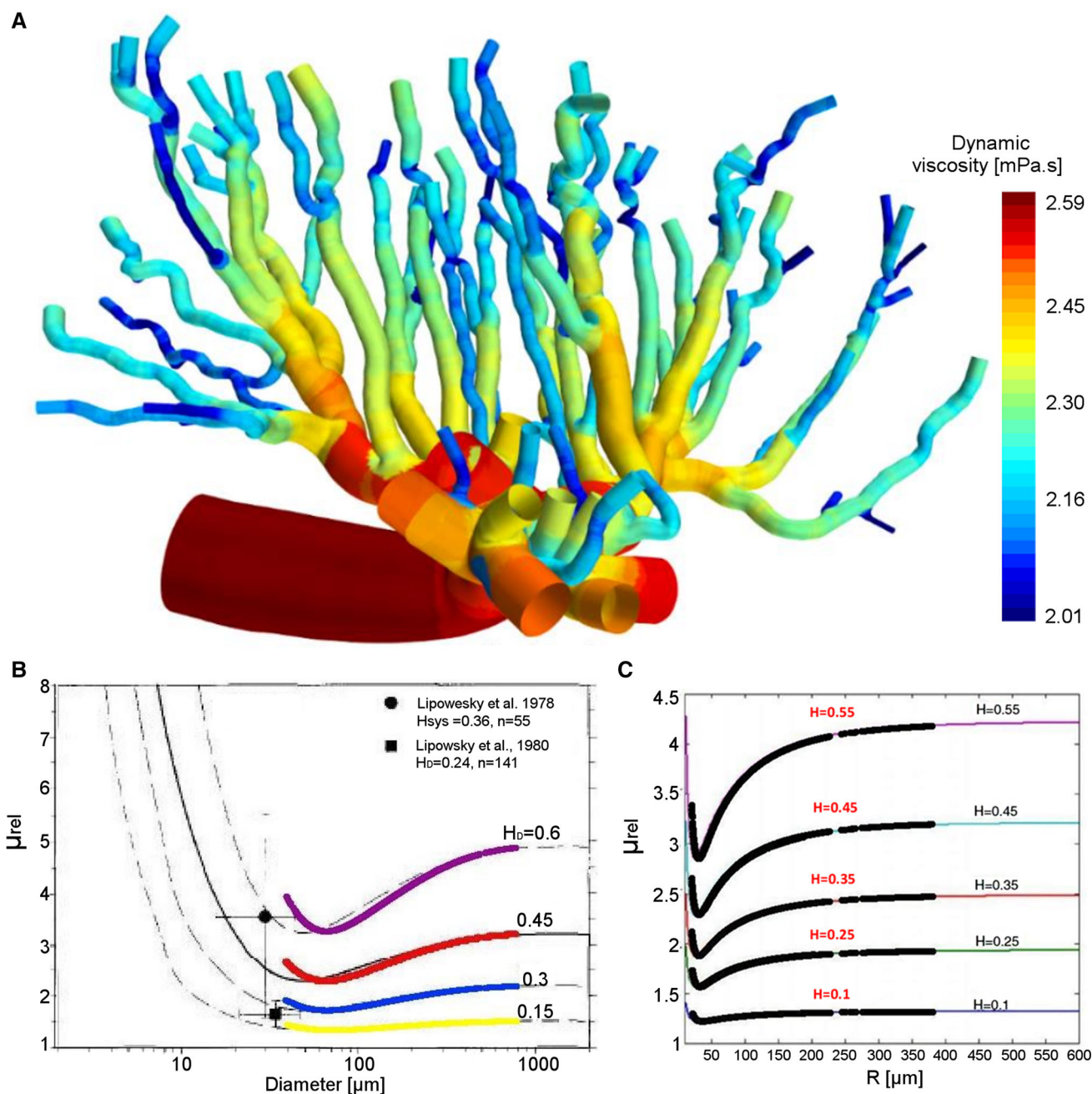
Fig. 2 **a** Dynamic viscosity of rat blood with a haematocrit of 31.7% and plasma viscosity of 1.1 mPa s with the Fåhræus–Lindqvist effect. **b** Comparison of relative viscosities computed with our model of the Fåhræus–Lindqvist effect (shown in *colour* for each haematocrit value) to in vivo measurements (Pries et al. 1996 and references within). **c** Our data (shown in *black*) compared to 2D simulations (Malek et al. 2015) with varying haematocrit concentrations

ence in viscosity between the Fåhræus–Lindqvist effect and both Newtonian (see Fig. 3a) and non-Newtonian Carreau–Yasuda (see Fig. 3b) models shows the largest difference in smaller vessels (also as expected). However, the percentage difference was more pronounced when comparing the Fåhræus–Lindqvist effect with the Carreau–Yasuda model (see Fig. 3b). As shown in Fig. 2, larger relative viscosities are observed in larger vessels. The overall Fåhræus–Lindqvist

viscosity is calculated by multiplying the relative viscosity by the plasma viscosity, implying that in larger vessels the blood viscosity approaches the absolute Newtonian viscosity. We can deduce that the Carreau–Yasuda model fails to account for the formation of the red blood cell core and plasma cell-free layer, and therefore does not resemble the biophysical behaviour of blood in the microvasculature.
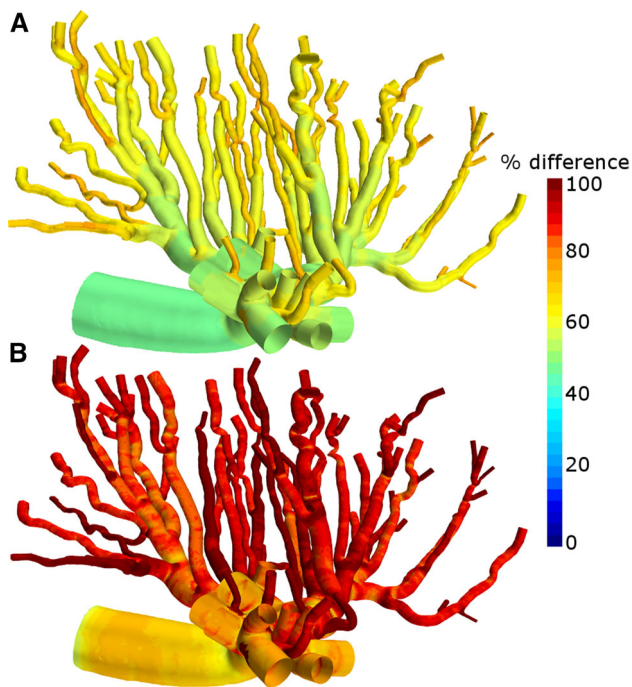
Fig. 3 Percentage differences in viscosity between the Fåhræus–Lindqvist effect and **a** Newtonian and **b** non-Newtonian Carreau–Yasuda models

3.3 Wall shear stress in the feto-placental network

Here we show for the first time the variation in WSS along feto-placental vessel segments, which indicates potential variations in signalling and remodelling (see Fig. 4). WSS differences were prominent at larger branching points such as the umbilical bifurcation where systolic flow is higher and WSS is expected to be greater. WSS in these areas is
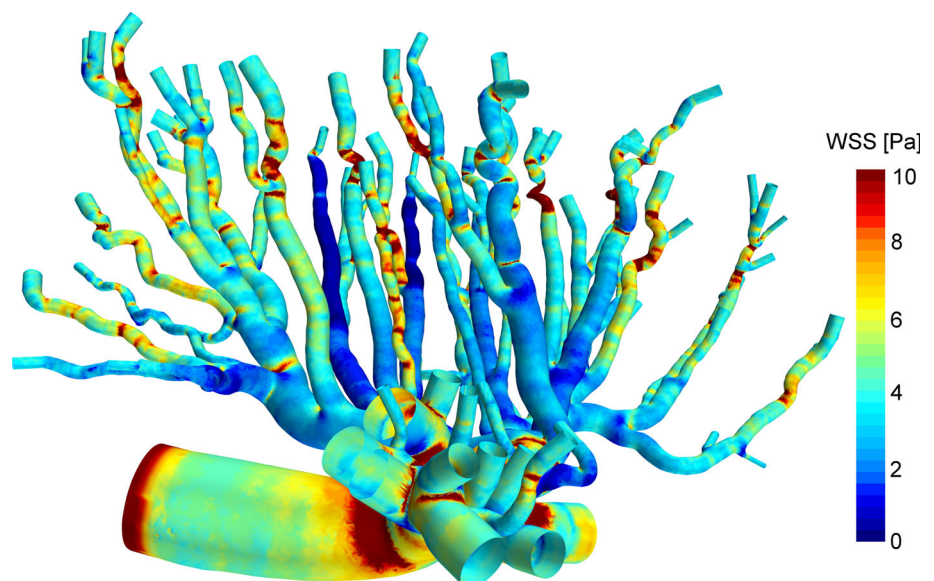
strongly associated with the activation of endothelial cell cascades which stimulate vascular remodelling and hence control the development of the hierarchical bifurcating tree structure (Barbee et al. 1995; Godde and Kurz 2001; Jones 2010).

High WSS (>10 Pa) creates unique transcriptional profiles in endothelial cells, promoting adaptive remodelling (Dolan et al. 2012). As a result, the large biomechanical blood forces present in the umbilical bifurcation predominate the wall's internal forces, promoting the enlargement of the vessel (Guzman et al. 1997). This local enlargement is essential for the placenta to meet the increasing nutrient, gas and waste exchange needs of the fetus during late pregnancy. The WSS increases downstream in the network of some vessels (see Fig. 4), which may also be associated with vessel enlargement and increased vessel sprouting to increase the flow, surface area and ultimately, the exchange functionality of vascular beds. Furthermore, it is not sufficient to simply know the magnitude of blood flow reaching the capillaries, with the exact patterns of flow essential to further our understanding of the physiology (Faber 1995; Plitman Mayo et al. 2016). The data presented here help work towards this ultimate goal.

We find WSS peaks above 10 Pa, which is significantly larger than previous work that ranged from zero to about 4 Pa (Rennie et al. 2012; Yang et al. 2010). However, there are several key differences between previous work and this current study. Firstly, we used rats compared to mice (Rennie et al. 2012; Yang et al. 2010) and as rats are larger animals, they have larger umbilical artery diameters compared to mice (756 v 380 μm). Also, using the pressure-drop approach of Yang et al., they estimated flow rate in the largest mouse placental vessels to be approaching 10 mm³/s, compared to

Fig. 4 WSS distributions based on the Fåhræus–Lindqvist effect and rat blood viscosity. Peak WSS was above 10 Pa, and previous work has shown WSS >10 Pa to cause endothelial cells to express unique transcriptional profiles that induce arterial remodelling (Dolan et al. 2012)

Fig. 5 a WSS magnitude and **b** WSS gradient distributions at the umbilical artery bifurcation based on the Fåhræus–Lindqvist effect and determined rat blood viscosity
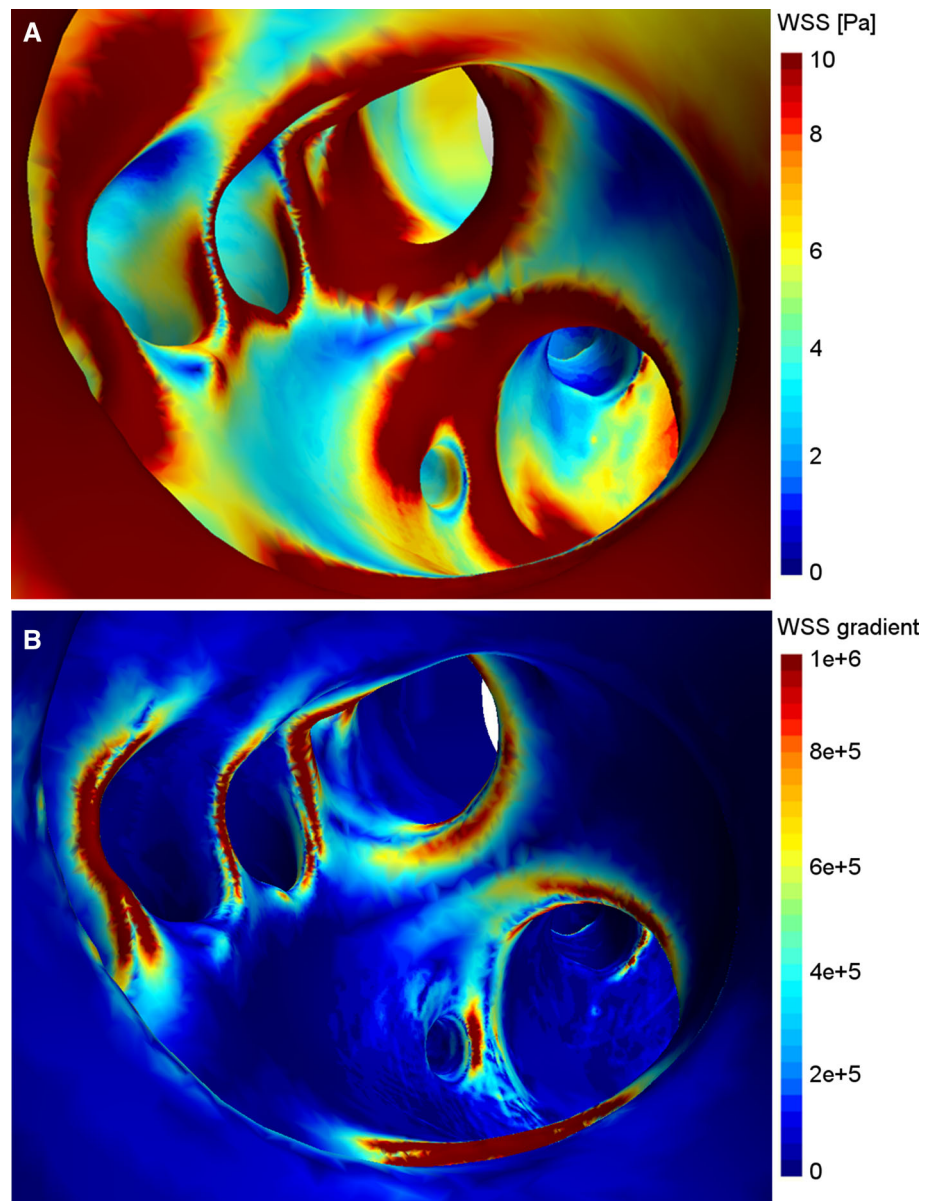
the average peak flow rate of 61.2 mm³/s measured using ultrasound in our rats. Therefore, the difference in species helps explain the differences in resulting WSS.

Here, we reveal the WSS gradients within specific segments of the feto-placental arterial network and in particular, within the umbilical artery bifurcation (see Fig. 5). We observe local WSS minimum at the bifurcation point experiencing flow impingement, with increasing WSS on either flank. Furthermore, we see WSS decreasing distally into the daughter branches, causing a positive WSS gradient at the entrance to these branching arteries. Dolan et al. (2013) investigated differential gene expressions by endothelial cells under varying streamwise gradients of WSS within the basilar terminus of rabbits. They showed that positive WSS gradients favour in vitro proliferation, apoptosis and extracellular matrix degradation, while decreasing the expression of pro-inflammatory genes. When genes Ki-67 and ADAMTS1 were activated, they were strongly associated with vascular remodelling processes such as cellular proliferation and extracellular matrix degradation. By mapping the immunofluorescence staining for the proliferation marker Ki-67 and ADAMTS1, they revealed a higher expression of the proliferation genes in endothelial cells experiencing positive WSS gradients compared to adjacent regions of negative WSS gradients (Dolan et al. 2013). Therefore, the WSS gradients we show here could be pivotal to vascular remodelling at bifurcations and in branching vessels.

3.4 Limitations of the study

Firstly, due to the computational size of the model, we did not simulate haemodynamics throughout the full feto-placental network. Instead we selected approximately one-third of the geometry. With further work, the entire network could be prepared for CFD similar to the excellent prior work in the area (Rennie et al. 2011, 2015, 2014, 2007; Yang et al. 2010). This could be achieved using automated methods to trim vessels as previously reported (Yang et al. 2010). We also are currently using advanced μCT imaging to connect the feto-placental arteries with the capillary network to create a highly sophisticated geometry that combines our 3D haemodynamic simulations with oxygen transfer in the capillaries (Pearce et al. 2016; Plitman Mayo et al. 2016).

Despite the extensive use of rodent models in haemodynamic studies, there is a knowledge gap in rat blood rheology, in particular, in rat fetal blood viscosity. We have estimated values by reviewing and extracting data previously published, but ultimately, experimental data are needed to support our findings.

Here, we used high-frequency Doppler ultrasound to measure the velocity in the umbilical artery of pregnant rats. However, instead of using this data to create a transient velocity input, we averaged the peak systolic velocity data and applied a steady-state inlet velocity to our model. Pulsatile simulations will significantly increase the computational times, but will create more accurate transient data allowing for WSS to be averaged over a cardiac cycle. Furthermore, a structured fractal tree (Kristen et al. 2016; Olufsen et al. 2000) or resistor boundary conditions could be implemented at the outlets to enhance the model. We aim to pursue these advancements to further refine our methodology in future work. Also, in vivo experimental validation is desirable. We will continue to explore methods of validation similar to those possible in larger arteries of the mouse (Feintuch et al. 2007) and also using future experimental data on oxygen tranfser and other physiological measurements.

Finally, the applicability of our findings to the human placenta is unclear. Although rodents are a valuable research tool and their placentas share geometric and physiological similarities with those of humans (Georgiades et al. 2002; Mu and Adamson 2006; Rennie et al. 2014; Wyrwoll et al. 2012; Yang et al. 2010), the imaging and modelling of human placental networks will also be useful and is under investigation by our group. Once adequate 3D imaging of a human network is acquired, a similar framework to that presented here can be applied and WSS computed.

4 Conclusions

Here, we present the first subject-specific 3D CFD model of the rat feto-placental network. We created a physiological estimate of rat fetal blood and used high-frequency Doppler ultrasound to measure velocity in the umbilical artery. We demonstrate the importance of the Fåhræus–Lindqvist effect and show that WSS is heterogeneous within the feto-placental network, with WSS gradients potentially creating important developmental pathways through gene expression that may contribute to vessel enlargement, sprouting and pruning. This work represents a significant advancement to our understanding of rat feto-placental haemodynamics and is a platform to help further investigate developmental haemodynamics in animals and humans.

References

Adamson SL, Lu Y, Whiteley KJ, Holmyard D, Hemberger M, Pfarrer C, Cross JC (2002) Interactions between trophoblast cells and the maternal and fetal circulation in the mouse placenta. Dev Biol 250:358–373. doi:10.1006/dbio.2002.0773

Barbee KA, Mundel T, Lal R, Davies PF (1995) Subcellular distribution of shear stress at the surface of flow-aligned and nonaligned endothelial monolayers. Am J Physiol 268:H1765–H1772

Bernard ES, Craina M, Bernard SI (2013) Hemodynamics of human placenta. WIT Trans Biomed Health 17:39–48. doi:10.2495/BIO130041

Burton GJ, Jauniaux E (1995) Sonographic, stereological and Doppler flow velocimetric assessments of placental maturity. Br J Obstet Gynaecol 102(10):818–825

Burton GJ, Charnock-Jones DS, Jauniaux E (2009) Regulation of vascular growth and function in the human placenta. Reproduction 138:895–902. doi:10.1530/REP-09-0092

Celik IB, Ghia U, Roache PJ, Freitas CJ, Coleman H, Raad PE (2008) Procedure for estimation and reporting of uncertainty due to discretization in CFD applications. J Fluids Eng 130:1–4

Clark AR, Lin M, Tawhai M, Saghian R, James JL (2015) Multiscale modelling of the feto-placental vasculature. Interface Focus 5:20140078. doi:10.1098/rsfs.2014.0078

Detmar J, Rennie MY, Whiteley KJ, Qu D, Taniuchi Y, Shang X, Casper RF, Adamson SL, Sled JG, Jurisicova A (2008) Fetal growth restriction triggered by polycyclic aromatic hydrocarbons is associated with altered placental vasculature and AhR-dependent changes in cell death. Am J Physiol Endocrinol Metab 295:E519–530. doi:10.1152/ajpendo.90436.2008

Dolan JM, Sim FJ, Meng H, Kolega J (2012) Endothelial cells express a unique transcriptional profile under very high wall shear stress known to induce expansive arterial remodeling. Am J Physiol Cell Physiol 302:C1109–C1118. doi:10.1152/ajpcell.00369.2011

Dolan JM, Meng H, Sim FJ, Kolega J (2013) Differential gene expression by endothelial cells under positive and negative streamwise gradients of high wall shear stress. Am J Physiol Cell Physiol 305:C854–866. doi:10.1152/ajpcell.00315.2012

Faber JJ (1995) Review of flow limited transfer in the placenta. Int J Obstet Anesth 4(4):230–237. doi:10.1016/0959-289X(95)82916-X

Fåhræus R, Lindqvist T (1931) The viscosity of the blood in narrow capillary tubes. Am J Physiol 96:562–568

Feintuch A, Ruengsakulrach P, Lin A, Zhang J, Zhou YQ, Bishop J, Davidson L, Courtman D, Pearce Foster FS, Steinman DA, Henkelman RM, Ethier CR (2007) Hemodynamics in the mouse aortic arch as assessed by MRI, ultrasound, and numerical modeling. Am J Physiol Heart Circ Physiol 292:H884–892. doi:10.1152/ajpheart.00796.2006

Georgiades P, Ferguson-Smith AC, Burton GJ (2002) Comparative developmental anatomy of the murine and human definitive placentae. Placenta 23:3–19. doi:10.1053/plac.2001.0738

Godde R, Kurz H (2001) Structural and biophysical simulation of angiogenesis and vascular remodeling. Dev Dyn 220:387–401. doi:10.1002/dvdy.1118

Gordan Z, Eytan O, Jaffa AJ, Elad D (2007) Fetal blood flow in branching models of the chorionic arterial vasculature. Ann NY Acad Sci 1101:250–265. doi:10.1196/annals.1389.037

Guzman RJ, Abe K, Zarins CK (1997) Flow-induced arterial enlargement is inhibited by suppression of nitric oxide synthase activity in vivo. Surgery 122:273–279. (discussion 279–280). doi:10.1016/S0039-6060(97)90018-0

Honda T, Honda K, Kokubun C, Nishimura T, Hasegawa M, Nishida A, Inui T, Kitamura K (2008) Time-course changes of hematology and clinical chemistry values in pregnant rats. J Toxicol Sci 33:375–380. doi:10.2131/jts.33.375

Jones EAV (2010) Mechanotransduction and blood fluid dynamics in developing blood vessels. Can J Chem Eng 88:136–143. doi:10.1002/cjce.20290

Kristen A, Kelsey LJ, Wintermantel E, Doyle BJ (2016) Fundus image based blood flow simulation of the retinal arteries. In: Joldes GR, Doyle BJ, Miller K, Wittek A, Nielson PMF (eds) Computational biomechanics for medicine: imaging, modelling and computing, vol 7. Springer, New York, pp 143-154. doi:10.1007/978-3-319-28329-6_13

Lecarpentier E, Bhatt M, Bertin GI, Salomon L, Deleron P, Fournier T, Barakat AI, Tsatsaris V (2016) Computational fluid dynamic simulations of maternal circulation: wall shear stress in the human placenta and its biological implications. PLoS ONE 11:e0147262. doi:10.1371/journal.pone.0147262

Lipowsky HH, Kovalcheck S, Zweifach BW (1978) The distribution of blood rheological parameters in the microcirculation of cat mesentery. Circ Res 43:738–749. doi:10.1161/01.RES.43.5.738

Lipowsky HH, Usami S, Chein S (1980) In vivo measurements of 'apparent viscosity' and microvessel hematocrit in the mesentery of the cat. Microvasc Res 19:297–319. doi:10.1016/0026-2862(80)90050-3

Linderkamp O (2004) Blood viscosity of the neonate. NeoReviews 5:e406–e416. doi:10.1542/neo.5-10-e406

Linderkamp O, Versmold HT, Riegel KP, Betke K (1984) Contributions of red cells and plasma to blood viscosity in preterm and full-term infants and adults. Pediatrics 74:45–51

Malek J, Azar AT, Nasralli B, Tekari M, Kamoun H, Tourki R (2015) Computational analysis of blood flow in the retinal arteries and veins using fundus image. Comp Math Appl 69:101–116. doi:10.1016/j.camwa.2014.11.017

Mu J, Adamson SL (2006) Developmental changes in hemodynamics of uterine artery, utero- and umbilicoplacental, and vitelline circulations in mouse throughout gestation. Am J Physiol Heart Circ Physiol 291(3):H1421–1428. doi:10.1152/ajpheart.00031.2006

Olufsen MS, Peskin CS, Kim WY, Pedersen EM, Nadim A, Larsen J (2000) Numerical simulation and experimental validation of blood flow in arteries with structured-tree outflow conditions. Ann Biomed Eng 28:1281–1299. doi:10.1114/1.1326031

Pearce P, Brownhill P, Janacek J, Jirkovska M, Kubinova L, Chernyavsky IL, Jensen OE (2016) Image-based modeling of blood flow and oxygen transfer in feto-placental capillaries. PLoS ONE 11(10):e0165369. doi:10.1371/journal.pone.0165369

Plitman Mayo R, Olsthoon J, Charnock-Jones DS, Burton GJ, Oyen ML (2016) Computational modeling of the structure-function relationship in human placental terminal villi. J Biomech 49:3780–3787. doi:10.1016/j.biomech.2016.10.001

Pries AR, Secomb TW, Gebner T, Sperandio MB, Gross JF, Gaehtgens P (1994) Resistence to blood flow in microvessels in vivo. Circ Res 75:904–915. doi:10.1161/01.RES.75.5.904

Pries AR, Secomb TW, Gaehtgens P (1996) Biophysical aspects of blood flow in the microvasculature. Cardiovasc Res 32:654–667. doi:10.1016/S0008-6363(96)00065-X

Rennie MY, Detmar J, Whiteley KJ, Jurisicova A, Adamson SL, Sled JG (2012) Expansion of the fetoplacental vasculature in late gestation is strain dependent in mice. Am J Physiol Heart Circ Physiol 302:H1261–1273. doi:10.1152/ajpheart.00776.2011

Rennie MY, Detmar J, Whiteley KJ, Yang J, Jurisicova A, Adamson SL, Sled JG (2011) Vessel tortuousity and reduced vascularization in the fetoplacental arterial tree after maternal exposure to polycyclic aromatic hydrocarbons. Am J Physiol Heart Circ Physiol 300:H675–684. doi:10.1152/ajpheart.00510.2010

Rennie MY, Rahman A, Whiteley KJ, Sled JG, Adamson SL (2015) Site-specific increases in utero- and fetoplacental arterial vascular resistance in eNOS-deficient mice due to impaired arterial enlargement. Biol Reprod 92:48. doi:10.1095/biolreprod.114.123968

Rennie MY, Sled JG, Adamson SL (2014) Effects of genes and environment on the fetoplacental arterial microcirculation in mice revealed by micro-computed tomography imaging. Microcirculation 21:48–57. doi:10.1111/micc.12073

Rennie MY, Whiteley KJ, Kulandavelu S, Adamson SL, Sled JG (2007) 3D visualisation and quantification by microcomputed tomography of late gestational changes in the arterial and venous feto-placental vasculature of the mouse. Placenta 28:833–840. doi:10.1016/j.placenta.2006.12.005

Riopel L, Fouron JC, Bard H (1982) Blood viscosity during the neonatal period: the role of plasma and red blood cell type. J Pediatr 100:449–453

Roache PJ (1994) Perspective: a method for uniform reporting of grid refinement studies. J Fluids Eng 116:405–413. doi:10.1115/1.2910291

Roberts DJ, Post MD (2008) The placenta in pre-eclampsia and intrauterine growth restriction. J Clin Pathol 61:1254–1260. doi:10.1136/jcp.2008.055236

Soares MJ, Chakraborty D, Karim Rumi MA, Konno T, Renaud SJ (2012) Rat placentation: an experimental model for investigating the hemochorial maternal–fetal interface. Placenta 33:233–243. doi:10.1016/j.placenta.2011.11.026

Spiegel M, Redel T, Zhang YJ, Struffert T, Hornegger J, Grossman RG, Doerfler A, Karmonik C (2011) Tetrahedral vs. polyhedral mesh size evaluation on flow velocity and wall shear stress for cerebral hemodynamic simulation. Comp Meth Biomech Biomed Eng 14:9–22. doi:10.1080/10255842.2010.518565

Sprague B, Chesler NC, Magness RR (2010) Shear stress regulation of nitric oxide production in uterine and placental artery endothelial cells: experimental studies and hemodynamic models of shear stress forces on ednotherlial cells. Int J Dev Biol 54(2–3):331–339. doi:10.1387/ijdb.082832bs

Vitello DJ, Ripper RM, Fettiplace MR, Weinberg GL, Vitello JM (2015) Blood density is nearly equal to water density: a validation study of the gravimetric method of measuring intraoperative blood loss. J Vet Med 2015:152730. doi:10.1155/2015/152730

Whiteley KJ, Adamson SL, Pfarrer CD (2006) Vascular corrosion casting of the uteroplacental and fetoplacental vasculature in mice.

Methods Mol Med 121:371–392. doi:10.1385/1-59259-983-4:369

Wyrwoll CS, Kerrigan D, Holmes MC, Seckl JR, Drake AJ (2012) Altered placental methyl donor transport in the dexamethasone programmed rat. Placenta 33(3):220–223. doi:10.1016/j.placenta.2011.12.017

Yang J, Yu LX, Rennie MY, Sled JG, Henkelman RM (2010) Comparative structural and hemodynamic analysis of vascular trees. Am J Physiol Heart Circ Physiol 298:H1249–1259. doi:10.1152/ajpheart.00363.2009

Zhang S, Regnault TR, Barker PL, Botting KJ, McMillen IC, McMillan CM, Roberts CT, Morrison JL (2015) Placental adaptations in growth restriction. Nutrients 7:360–389. doi:10.3390/nu7010360